LANGMUIR

pubs.acs.org/Langmuir Article

Insights into Structural Behaviors of Thiolated and Aminated Reduced Graphene Oxide Supports to Understand Their Effect on MOR Efficiency

Minh Thu Vu, Thi Thanh Ngan Nguyen, Tran Quang Hung, Thuan-Nguyen Pham-Truong, Magdalena Osial, Philippe Decorse, Thi Thom Nguyen, Benoit Piro, and Vu Thi Thu*

Cite This: *Langmuir* 2023, 39, 13897−13907 Read Online

ACCESS | Metrics & More | Article Recommendations | Supporting Information

ABSTRACT: It is essential to develop novel catalysts with high catalytic activity, strong durability, and good stability for further application in methanol fuel cells. In this work, we present for the first time the effect of the chemical functional groups (thiol and amine) with different electron affinity in reduced graphene oxide supports on the morphology and catalytic activity of platinum nanoparticles for the methanol oxidation reaction. Hydroxyl groups on graphene oxide were initially brominated and then transformed to the desired functional groups. The good dispersion of metal nanoparticles over functionalized carbon substrates (particle size less than 5 nm) with good durability, even at a limited functionalization degree (less than 7%) has been demonstrated by morphological and structural studies. The durability of the catalysts was much improved via strong coordination between the metal and nitrogen or sulfur atoms. Impressively, the catalytic activity of platinum nanoparticles on aminated reduced graphene oxide was found to be much better than that on thiolated graphene oxide despite the weaker affinity between amine and noble metals. These findings support further developing new graphene derivatives with the desired functionalization for electronics and energy applications..

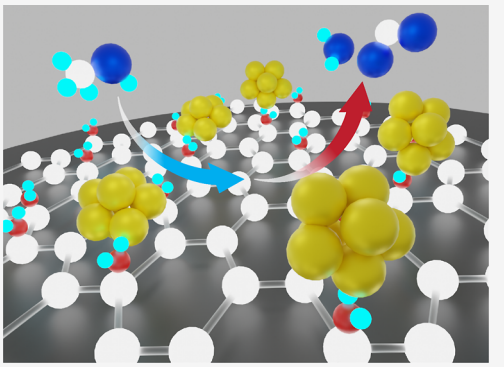

INTRODUCTION

Platinum nanoparticle (PtNP) is one of the most efficient catalysts for the methanol oxidation reaction (MOR) in fuel cells.[1] However, avoiding unexpected particle aggregation, which is not profitable for catalytic activity, is always challenging. The use of suitable supports such as carbon, conducting polymer, or organic film[2,3] might help to prevent the intrinsic accumulation of metal nanoparticles. For instance, H. Huang et al. have successfully assembled grain boundary—enriched PtNPs onto graphitic carbon or $Ti_3C_2T_x$ MXene nanosheets to provide catalysts with a superior methanol oxidation performance.[4,5] The durability and stability of these catalyst systems can be further improved via the strong attachment of metal nanoparticles to the support at anchoring sites containing electron donor centers with high affinity toward noble metals.[6−10]

The anchoring sites based on sulfur- or nitrogen-containing moieties can be introduced via chemical doping or functionalization of graphene flakes. In the former approach, the heteroatoms (S, N, O, P) are embedded in carbonaceous planes.[11−13] The replacement of carbon with doping atoms in the backbone could tune electrical behavior[14,15] or make the support become a metal-free catalyst[16−20] in some cases. It was recently reported that the surface corrugations such as nanoscale ripples might play a role in the catalytic activity of graphene.[21] In the latter approach, the desired functional groups (i.e., thiol and amine) are introduced onto carbon supports via chemical bonds directly to carbon atoms on graphene flakes.[22] Since chemical functionalization is often conducted through well-known chemical reactions, the generation of unexpected functional groups (i.e., thiols, SO_3, sulfur-epoxy, thiophene in S-doped graphene) can be actually avoided.[23,24] At the same time, the damage in the structure of the graphite domains in chemical functionalization is much less than that in the chemical doping process, in which high temperature is often required. The most interesting thing is that we can eventually decorate the graphene sheets with desired molecules via these functional groups.

Few research groups have worked on thiolation, whereas many others have studied the amination of graphene derivatives. Rourke et al. have reported the attachment of reactive thiol functional groups to positions of epoxide groups

Received: May 29, 2023
Revised: September 12, 2023
Published: September 22, 2023

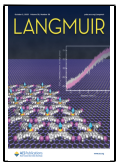

in graphene oxide via epoxide ring-opening.[25] Later on, Pumera and Kiang have shown a one-pot monothiolation and reduction of graphene oxide at both epoxide and hydroxyl sites.[26] It has been demonstrated that this procedure provides more active sites. On the other hand, for introduction of amine functions, The Leuckart reaction is one standard reductive amination method that enables both reduction of graphene oxide and introduction of primary amine at carbonyl groups.[27] Using Hoffman rearrangement, it is also possible to directly replace the carboxylic groups at the edges of graphite flakes with amine groups.[28] It can be noticed that the degree of amination in these methods is not very high since the amination mainly occurs at the edges of graphite flakes. Recently, Kirilenko and his co-workers have reported a simultaneous reduction and amination process via treatment with hydrobromic acid and ammonia.[29] Since the reactions happen at basal plane groups (hydroxyl and epoxy) in mild conditions, it is expected to provide a considerable amination degree of up to 4 at. %.

The aim of this work is to understand how the two functional groups, i.e. amine and thiol, with different electron affinities will affect the catalytic activity and durability of functionalized graphene sheets decorated with platinum particles. We will first prepare aminated and thiolated reduced graphene oxide using the simultaneous reduction and functionalization method as mentioned by Pumera and Kirilenko.[26,29] In principle, graphene oxide is converted to brominated reduced graphene oxide before the bromide is replaced with an amine or a thiol group. PtNPs will then be decorated onto functionalized reduced graphene oxide via polyol reduction. The catalytic activity toward MOR of the final products will be investigated in an alkaline solution using different electrochemical methods.

EXPERIMENTAL SECTION

Materials. Natural graphite powder (flake size less than 20 μm), sulfuric acid (H_2SO_4 95−98%), hydrochloric acid (HCl 37%), sodium nitrate ($NaNO_3$), potassium permanganate ($KMnO_4$), hydrogen peroxide (H_2O_2 30%), hydrobromic acid (HBr 48%), thiourea (CH_4N_2S), sodium hydroxide (NaOH), ammonia solution (NH_4OH), chloroform ($CHCl_3$), isopropyl alcohol (C_3H_8O), ethylene glycol (EG), and chloroplatinic acid hydrate ($H_2PtCl_6{\cdot}xH_2O$) were purchased from Sigma-Aldrich. Methanol (CH_3OH) and ferrocyanide $Fe(CN)_6^{3-/4-}$ redox probes were also supplied by Sigma-Aldrich. Deionized water was used for washing graphene materials. Argon (Ar) with 99% purity was used to purge the solution. Graphene oxide (GO) was prepared by Hummers' method as described in our previous studies.[30]

Preparation of Thiolated Reduced Graphene Oxide. Thiolation and reduction of GO flakes were processed as described in the previously reported work.[26] Typically, a mixture of 15 mL of aqueous dispersion of GO (1 mg mL^{-1}) and 1 mL of HBr (48%) was prepared and stirred at 30 °C for 2 h. One g of thiourea was then added to the mixture, and the reaction proceeded at 80 °C for 24 h. After that, the solution was cooled down to room temperature before adding 10 mL of NaOH 4 M. After 30 min, the mixture was repeatedly washed with deionized water and centrifuged. The collected solid was dried at 40 °C under reduced pressure overnight to provide the final product so-called GSH sample.

Preparation of Aminated Reduced Graphene Oxide. The brominated reduced graphene oxide (prepared as mentioned in the previous section) was washed several times using isopropyl alcohol solvent and then collected via centrifugation (10,000 rpm, 30 min) to get a black sediment. This sediment was then mixed with a saturated solution of ammonia in isopropyl alcohol, and the mixture was stirred by a magnetic stirrer for 1 h. The obtained product was washed again, and the final product so-called GNH was dried in a vacuum oven at 50 °C overnight.

Preparation of PtNPs on Carbon Supports Using Polyol Reduction. PtNPs were decorated onto carbon supports (graphene oxide, thiolated, and aminated graphene oxide) via the polyol reduction process. A specific amount of carbon support (30 mg) was dispersed in 20 mL of ethylene glycol by ultrasonic treatment until a black homogeneous solution with solid content of 1.5 mg mL^{-1} was obtained. The yellow solution of chloroplatinic acid H_2PtCl_6 in ethylene glycol was prepared at the same concentration (1.5 mg mL^{-1}). Carbonaceous dispersion was then transferred to a three-neck round-bottom flask with argon flowing for 30 min. The system was then heated up to 140 °C. After that, a solution of H_2PtCl_6 in ethylene glycol was added, and the reaction mixture was stirred for 4 h before being cooled to room temperature. During the process, ethylene glycol was used as both solvent and reducing agent; and $H_2PtCl_6{\cdot}xH_2O$ was used as the platinum precursor. The obtained black mixture was washed and centrifuged with deionized water five times at 10,000 rpm for 30 min. The product was finally dried in a vacuum oven at 50 °C for 24 h. The final catalysts based on GO, GSH, and GNH supports were named G@PtNPs, GSH@PtNPs, and GNH@PtNPs, respectively.

Morphological and Structural Studies. Field emission scanning electron microscopy (SEM) images were captured on a S-4800 system (Hitachi, Japan) operated at a 5 kV accelerating voltage to study the morphology of as-synthesized samples. SEM was equipped with an energy-dispersive X-ray spectroscope to evaluate the elemental composition. The morphology of the samples was also investigated using transmission electron microscopy (TEM)—Zeiss Libra 120 Plus, Stuttgart, Germany, operating at 120 kV. Samples were placed from the aqueous suspension on the copper mesh (300 grids) coated with the Formvar layer.

Structural behavior was studied with Fourier transform infrared (FTIR) spectroscopy using a Nicolet iS50 FTIR spectrometer (Thermo-Fisher, USA). The crystalline structure of the powder samples was verified by Raman spectroscopy with a LabRAM Raman system (HORIBA, Japan) using 532 nm excitation. The band gap was determined with UV−vis spectra recorded using a UV-1280 spectrometer (Shimadzu, Japan) in the visible range (300−800 nm). The binding states of elements were revealed from X-ray photoelectron spectroscopy (XPS) spectra recorded on a PHI Versa Probe III XPS system (ULVAC-PHI) using a monochromatized Al−K X-ray source (1486.6 eV DTA-DSC). The active surface area of the samples was estimated from nitrogen adsorption−desorption curves recorded on a Tristar-3030 system (Micromeritics-USA) at 77 K using the Brunauer−Emmett−Teller (BET) method. Zeta potential of the samples was measured on a zeta potential analyzer from HORIBA.

Electrochemical Behaviors. All electrochemical experiments were performed in a 10 mL electrochemical cell at room temperature using a three-electrode configuration with an AUTOLAB 302N workstation (Metrohm, the Netherlands). Glassy carbon electrodes (diameter 3 mm) were used as working electrodes (bare or modified), Ag|AgCl|3 M KCl electrodes as reference electrodes, and Pt wires as counter electrodes. To evaluate electron transfer at the electrode surface, the cyclic voltammograms were recorded for three cycles in the potential range of −0.3 to 0.8 V at a scan rate of 50 mV s^{-1} in 100 mM KCl solution containing 5 mM $Fe(CN)_6^{3-/4-}$ redox probe. The charge-transfer resistance was also investigated through the electrochemical impedance spectroscopy technique between a frequency range of 10^5 and 10^{-1} Hz and an applied voltage of 0.19 V in the same redox solution.

The electrochemically active surface area (ECSA) of the electrode surfaces was determined from cyclic voltammograms recorded in degassed H_2SO_4 0.5 M solution at room temperature with potentials between −0.6 and 1.5 V at a scan rate of 50 mV s^{-1}. The values of the ECSA and the amount of the Pt catalyst (m_{Pt}) in the samples can be estimated as follows[5,31]

$$m_{Pt} = \frac{Q_H M}{4F}$$

https://doi.org/10.1021/acs.langmuir.3c01446
Langmuir 2023, 39, 13897−13907

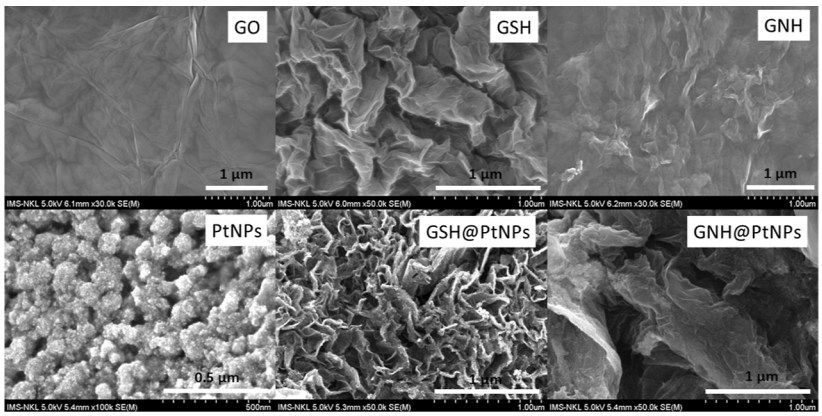

Figure 1. SEM images of GO, GSH, GNH, PtNP, GSH@PtNP, and GNH@PtNP samples.

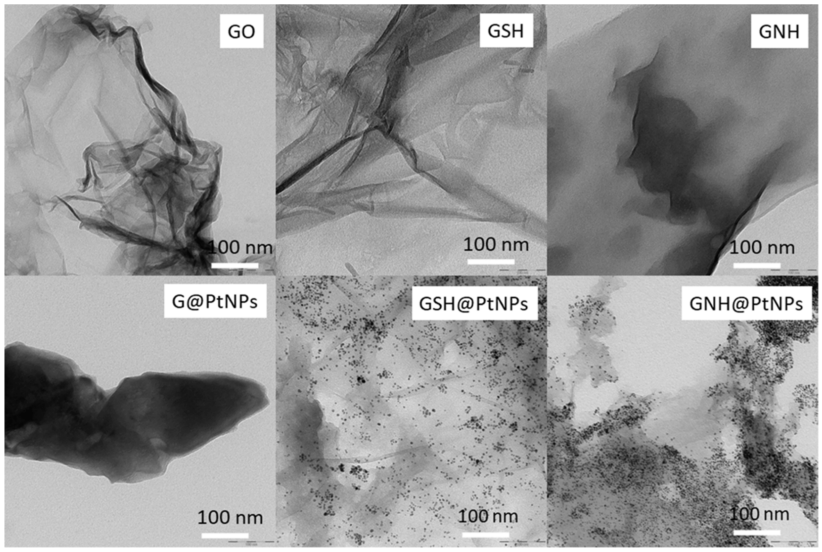

Figure 2. TEM images of GO, GSH, GNH, G@PtNP, GSH@PtNP, and GNH@PtNP samples.

$$\text{ECSA} = \frac{Q_H\ (\mu C)}{m_{Pt} \times 210\ \mu C\ cm^{-2}}\ (m^2\ g^{-1})$$

where Q_H is the amount of charge that varies along the surface of Pt during the hydrogen adsorption−desorption process, M is the atomic weight of Pt (195.09 g mol^{-1}), and F is the Faraday constant (96485.309 C mol^{-1}).

MOR Test. The as-prepared materials (PtNPs, G@PtNPs, GSH@PtNPs, and GNH@PtNPs) were deposited onto a glassy carbon electrode (GCE) via a drop-casting method. Specifically, 5 μL of material dispersion with the solid content of 1 mg mL^{-1} was drop-casted on the bare electrode and then allowed to be dried at 60 °C for 10 min. The MOR test was carried out in solution of 10 mL of NaOH 0.5 M with different amounts of MeOH (0−200 μL) via cyclic voltammetry measurement with the potential range between −0.8 and 0.2 V/AglAgCl and at a scan rate of 50 mV s^{-1}.

RESULTS AND DISCUSSION

SEM and TEM Images. SEM images (Figure 1) were first captured to evaluate the effect of the carbon support on the dispersion of the metal nanoparticles. It can be seen that PtNPs were homogeneously dispersed at high density onto the carbon supports with a size of less than 10 nm. There is also no significant accumulation of metal nanoparticles as observed in PtNPs. These results might come from the fact that PtNPs have been in situ seeded and grown onto negatively charged graphite flakes (with abundant oxygen-containing functional groups) from a homogeneous salt solution. The presence of functional groups (thiol or amine) with high affinity toward PtNPs have even increased the number of nucleation sites to anchor more PtNPs, thus decreasing the particle size and increasing the density of metal nanoparticles on functionalized carbon supports. In addition, the flexible structure of carbon supports has additionally provided a large surface area for immobilizing metal nanoparticles.

The average particle size of PtNPs (evaluated from TEM images as seen in Figure 2) was found to be about an average of 4.6 nm for thiolated (GSH) and 3.2 nm for aminated reduced graphene oxide support (GNH). Histograms to show the size distribution of PtNPs on the catalysts are provided in Supporting Information (Figure S1). These values are very beneficial for catalytic performance and comparable with those reported for metal nanoparticles dispersed on reduced graphene oxide[15,32,33] or other carbon-based materials[9,34] in previous studies. As the solid samples needed to be well-dispersed in solvent for their drop-casting on the copper grids for further TEM analysis, it was also found that the metal nanoparticles on functionalized carbon supports stay more durable and stable compared to those on reduced graphene oxide.

https://doi.org/10.1021/acs.langmuir.3c01446
Langmuir 2023, 39, 13897−13907

XPS Analysis. The Pt loading yield on the carbon supports of the samples was assessed via XPS analysis (Table 1). As shown in Table 1, the amount of the metal catalyst in GSH@PtNPs (8.10 atom %) is 4.4 times higher than that in GNH@PtNPs (1.83 atom %) and 20.3 times higher than that in G@PtNPs (0.40%). Obviously, the loading amount of Pt element onto the carbon support should be highest in thiolated one due the high affinity between metal nanoparticles and the thiol functional group.[35,36] Similar results were also obtained from EDX analysis (Figure S2).

Table 1. XPS Analysis of GSH@PtNPs and GNH@PtNPs

sample	O/C ratio	Pt content (% at.)
GO	0.418	
GSH	0.124	
GNH	0.232	
G@PtNPs	0.293	0.40
GSH@PtNPs	0.184	8.10
GNH@PtNPs	0.226	1.83

More details on the binding states of elements in the samples are shown in deconvoluted XPS spectra. The S 2p deconvoluted XPS spectrum of GSH@PtNPs (Figure 3) shows peaks related to HS-C (S $2p_{3/2}$ at 164.1 eV, S $2p_{1/2}$ at 165.3 eV), RS-C (S $2p_{3/2}$ at 167.1 eV and S $2p_{1/2}$ at 168.3 eV), and SO_4^{2-} (S $2p_{3/2}$ at 169.6 eV and S $2p_{1/2}$ at 170.8 eV).[26] The intensity of the peak related to HS-C (thiol) was found to be dominant over other sulfur-containing functional groups such as RS-C (possibly from unhydrolyzed thiourea or unwanted sulfur-epoxy) and S−O (from SO_4^{2-} intercalated within graphite flakes). No evidence on the formation of the S−S bridge at low binding energies was observed on the XPS spectrum of GSH. It seems to be hard to make the bridge between sulfur atoms which are well-separated due to low sulfur content in the GSH sample. The N 1s deconvoluted XPS spectrum of GNH@PtNPs (Figure 3) shows two peaks relevant to C−N (399.4 eV) and C−NH^+ (401.4 eV). The thiolation degree in GSH@PtNPs (estimated from the ratio between S−C/total C) was 6.65%, whereas the amination degree in GNH@PtNPs (estimated from the ratio between N−C/total C) was found to be only 3.41%. The presence of Pt element in GSH@PtNPs and GNH@PtNPs was clearly demonstrated by the occurrence of the two typical peaks Pt 4f $_{5/2}$ and Pt 4f $_{7/2}$ in the region of 68−80 eV on the high-resolution Pt 4f spectra (Figure 3).

The intensity of the signal associated with hydroxylated carbon atoms (C−O at binding energy of 286.7 eV) was significantly reduced after amination and nearly disappeared after thiolation, as demonstrated in C 1s deconvoluted XPS spectra of GO, GNH, and GSH (Figure 4). This is evidence to show that the functionalization of carbon supports mainly occurs at the position of hydroxyl groups. At the same time, this is also a clear evidence of the reduction of graphene oxide flakes after functionalization.[28,37] This result is in accordance with the decrease in the O/C ratio by 3.37 times after thiolation and 1.80 times after amination (Table 1).

Band Structure. UV−vis absorption spectra of the samples were examined to provide more information about the electronic structure of as-prepared materials (Figure 5A). The spectrum recorded for the GO sample presents two absorption peaks at 228 and 305 nm which are attributed to $\pi \rightarrow \pi^*$ transition coming from sp^2 domains and $n \rightarrow \pi^*$ transition in carbonyl and carboxylic groups, respectively.[38,39] After thiolation, the peak related to $\pi \rightarrow \pi^*$ transition disappeared whereas the peak related to $n \rightarrow \pi^*$ transition was blue-shifted to 260 nm, indicating the reduction of graphene oxide during functionalization.[40,41] Nevertheless, the two

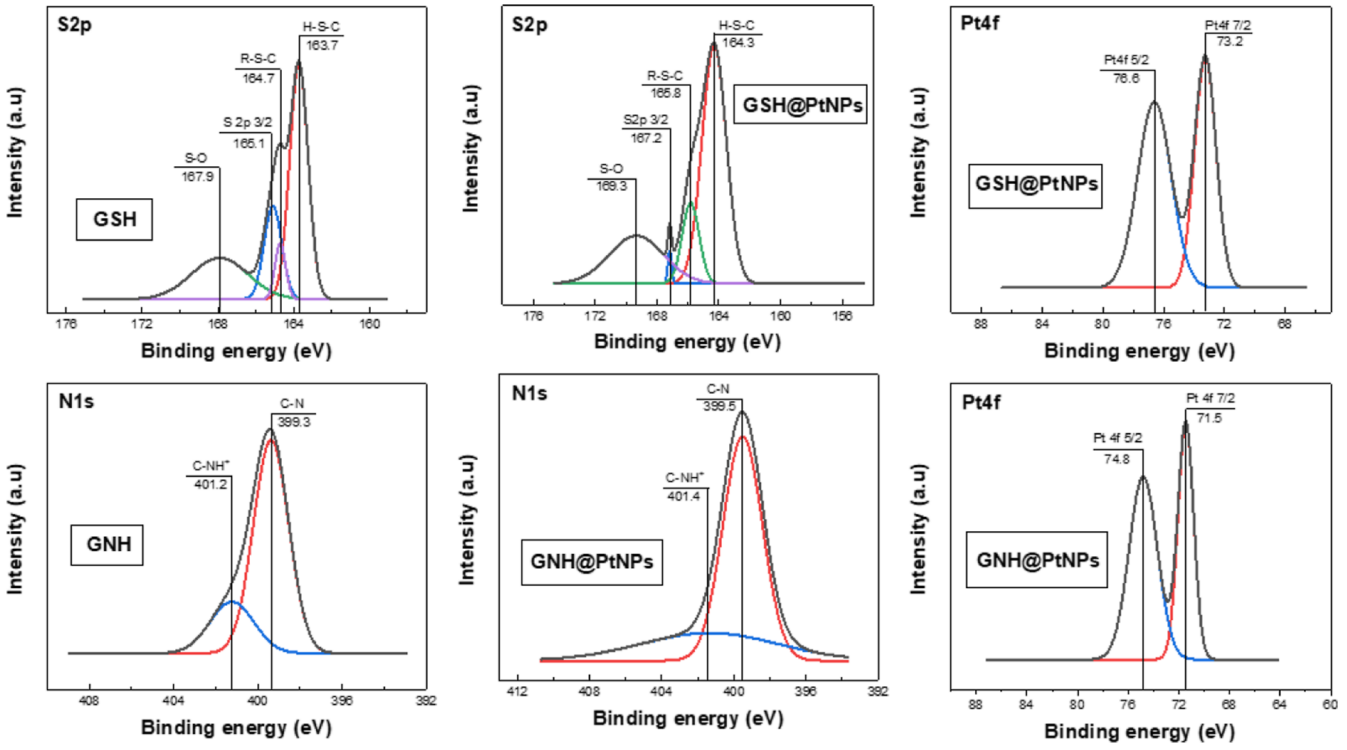

Figure 3. High-resolution C 1s spectra of graphene derivatives with and without PtNPs.

https://doi.org/10.1021/acs.langmuir.3c01446
Langmuir 2023, 39, 13897−13907

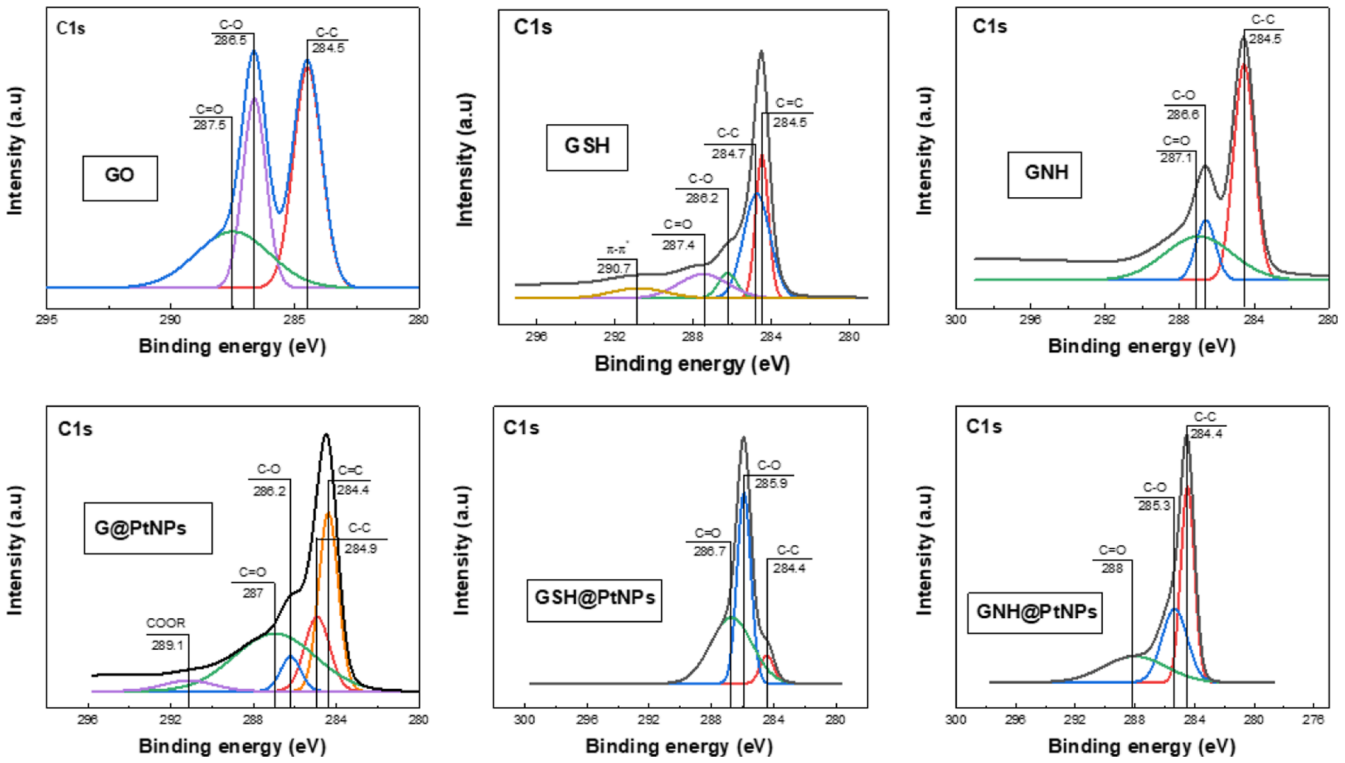

Figure 4. High-resolution S 2p and Pt 4f spectra of GSH@PtNPs and high-resolution N 1s and Pt 4f spectra of GNH@PtNPs.

transitions ($\pi \rightarrow \pi^*$ at 227 nm and $n \rightarrow \pi^*$ at 300 nm) still remained after amination. This result is in good agreement with our previous EDX and XPS analysis that the reduction degree of graphene oxide after thiolation is higher than amination. The plasmon absorption was found at 268 nm for PtNPs. This peak was shifted to shorter wavelengths at 263 nm for GNH@PtNPs and 260 nm for GSH@PtNPs. This result points out the decrease in the particle size once metal nanoparticles are dispersed onto carbon supports.

The energy band gap (estimated from Tauc plots in Figure S3) was also found to be shortened from 4.17 to 3.26 eV after thiolation and 3.82 eV after amination (Table 1). The smaller band gap obtained in functionalized reduced graphene oxide probably resulted from the lower content of oxygen moieties (see more details in EDX and XPS analyses above) and restoration of sp^2 carbon atoms.[42,43] Moreover, the decrease in the graphite domain (see FTIR and Raman analyses later) might partly contribute to narrowing band gaps in functionalized materials.[40] Although the reduction might not be complete yet and the band gap is still quite large (not in the common range 1−3 eV[38] for rGO applicable in electronic devices), the as-prepared functionalized reduced graphene oxide can still be utilized for our sensing applications in which they act only as supporting materials to well disperse metal nanoparticles. Furthermore, Lian et al. have reported that a large band gap can still be found in highly reduced graphene oxide due to hybridization between the in-plane p_{xy} orbitals of oxygen atoms and the out-of-plane p_z orbital of graphene.[44]

FTIR and Raman Analyses. More information on structural behaviors of the samples was revealed from FTIR analysis. As seen from FTIR spectra (Figure 5B), the absorbance peaks related to sulfur- and nitrogen-containing moieties are very weak. As mentioned previously, the functionalized sites are mainly located at the positions of the hydroxyl groups. Probably, the low amount of hydroxyl functional groups (compared to other oxygen moieties) in the GO precursor might be the reason for this limited functionalization degree. Some typical vibration modes of oxidized graphite flakes[43] such as a broad vibrational band of −OH stretching (~3462 cm^{-1}), C═O stretching band (~1617 cm^{-1}), and C−OH stretching band (~1394 cm^{-1}) were also observed in graphene oxide and thiolated and aminated reduced graphene oxide. It was also reported that the detection of thiol or amine functional groups with such a low functionalization degree is indeed very challenging.[25,26]

In Raman spectra (Figure 5C), two characteristic peaks relevant to the E_{2g} mode (G peak at higher wavenumber) and A_{1g} (D peak at lower wavenumber) were found. The position of the G peak was shifted to a lower wavenumber (1602 cm^{-1} in GO, 1595 cm^{-1} in GSH, 1577 cm^{-1} in GNH). In contrast, the position of the D peak was slightly shifted to a higher wavenumber (1346 cm^{-1} in GO, 1348 cm^{-1} in GSH, 1353 cm^{-1} in GNH) after chemical functionalization. The smaller values of full width at half-maximum of the D band were also observed in functionalized carbonaceous materials. These results have once more confirmed the reduction of GO after thiolation or amination.[26]

The level of defects in graphite materials can also be revealed from the I_D/I_G ratio. It was found that the I_D/I_G ratio was increased from 0.84 for GO to 1.32 for GSH and 0.92 for GNH (Table 1), indicating a highly defective structure[9] due to C═C bond breaking during the bromination process.[26] Such high level of defects is commonly found in functionalized carbonaceous materials.[10] At the same time, the size of graphite domain was reduced (Table 1) from 22.89 nm in GO to 14.56 nm in the GSH sample and 20.9 nm in the GNH sample (estimated using formula $L = \frac{2.4 \times 10^{-10} \lambda^4}{I_D / I_G}$ developed by Tuinstra and Koenig[45]). Similar results were obtained by

https://doi.org/10.1021/acs.langmuir.3c01446
Langmuir 2023, 39, 13897−13907

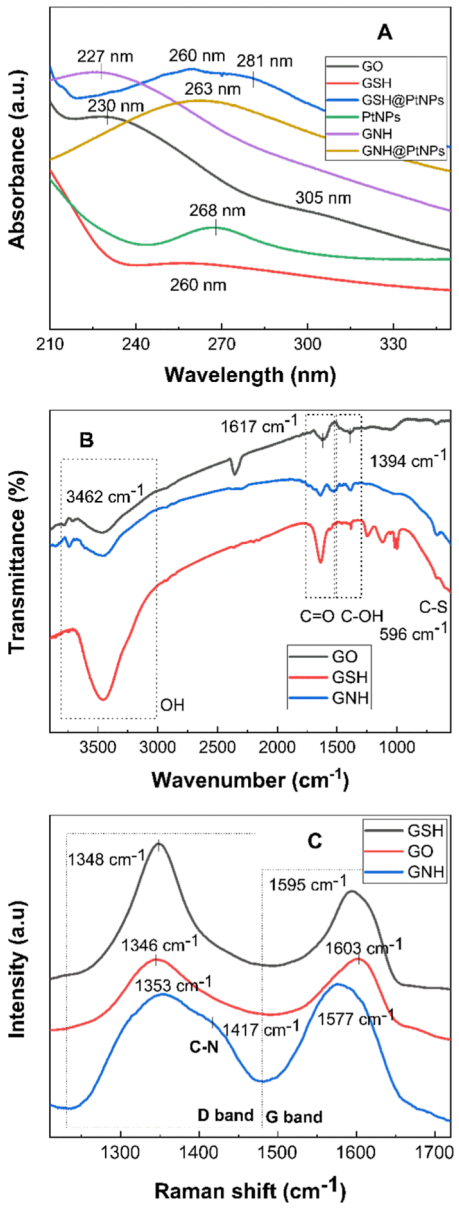

Figure 5. Structural characterization of graphene derivatives: UV−vis (A), FTIR (B), and Raman (C) spectra.

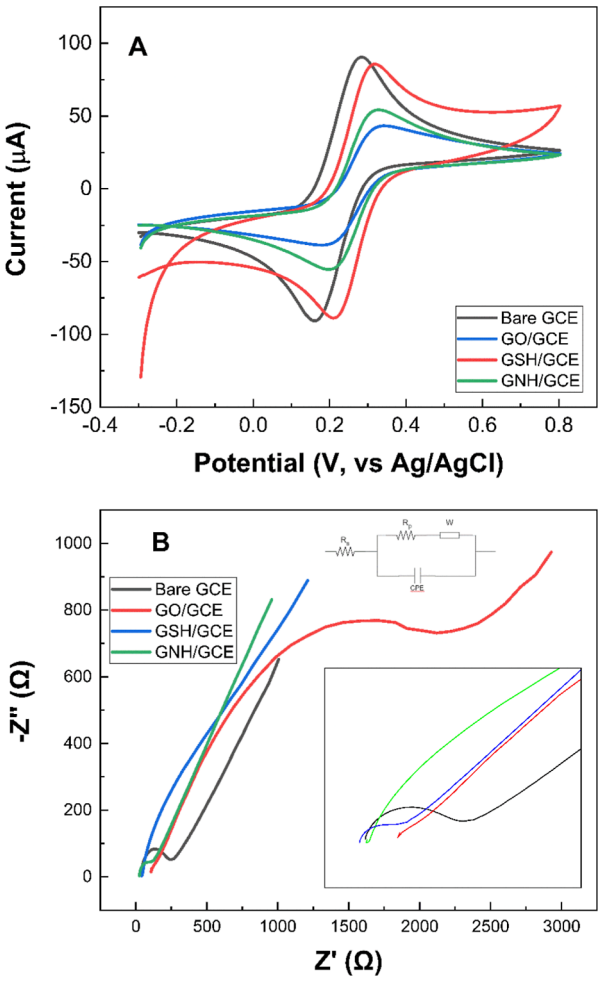

Figure 6. Electrochemical behaviors of graphene derivatives: cyclic voltammograms (A) and Nyquist plots (B) recorded in 100 mM KCl solution containing 5 mM $Fe(CN)_6^{3-/4-}$.

Pumera et al. during thiolation of GO due to the increase in proportion of sp^2 carbon atoms.[26] It is worth noticing that the higher reduction level is indeed accompanied by the higher defect level and smaller size of graphite domain in the GSH sample (compared to the GNH sample).

Electrochemical Studies. Electrochemical behaviors of the carbon-based materials (GO, GSH, GNH) were tested by recording cyclic voltammograms in a redox probe solution (Figure 6). Cyclic voltammograms have shown a reasonable electron transfer rate on electrodes modified with thiolated or aminated reduced graphene oxide with relatively narrow peak-to-peak separation (110 mV for GSH, 120 mV for GNH) which is lower than that in the GO modified electrode (138 mV) and bare electrode (124 mV). Even though the electron transfer rate at the surface of GSH or GNH is not extremely high, it is still sufficient to avoid the blocking effect at the electrode surface for further electrochemical applications.

MOR Test. Cyclic voltammetry measurements were recorded to investigate the MOR activity of the electrodes modified with PtNPs, G@PtNPs, GSH@PtNPs, and GNH@PtNPs in 0.5 M NaOH solution containing 0.1 M MeOH (Figure 9A). Based on the lack of an oxidation peak of the methanol in the cyclic voltammograms recorded on GSH/GCE and GNH/GCE, it can be concluded that thiolated or aminated reduced graphene oxide does not take part in the methanol oxidation process. For electrodes modified with PtNPs, G@PtNPs, GSH@PtNPs, and GNH@PtNPs, one peak in forward scan (methanol oxidation) and one peak in backward scan (oxidation of oxidative intermediates) on cyclic voltammograms were recorded in methanol solution.[5] The occurrence of methanol oxidation peak in the cyclic voltammograms recorded on G@PtNPs/GCE, GSH@PtNPs/GCE, and GNH@PtNPs/GCE in methanol solution is indeed an indicator of a successful decoration of PtNPs on the carbon supports. Compared with PtNP-modified GCE, the current responses recorded on the PtNP-functionalized carbon supports were much improved. Consequently, the mass activity and surface activity of the catalysts were much improved as seen in Supporting Information (Figure S7). The use of carbon supports must have helped to improve the dispersion of PtNPs and reduced the possibility of obtaining aggregated PtNPs. Furthermore, the abundant number of nitrogen- or sulfur-

https://doi.org/10.1021/acs.langmuir.3c01446
Langmuir 2023, 39, 13897−13907

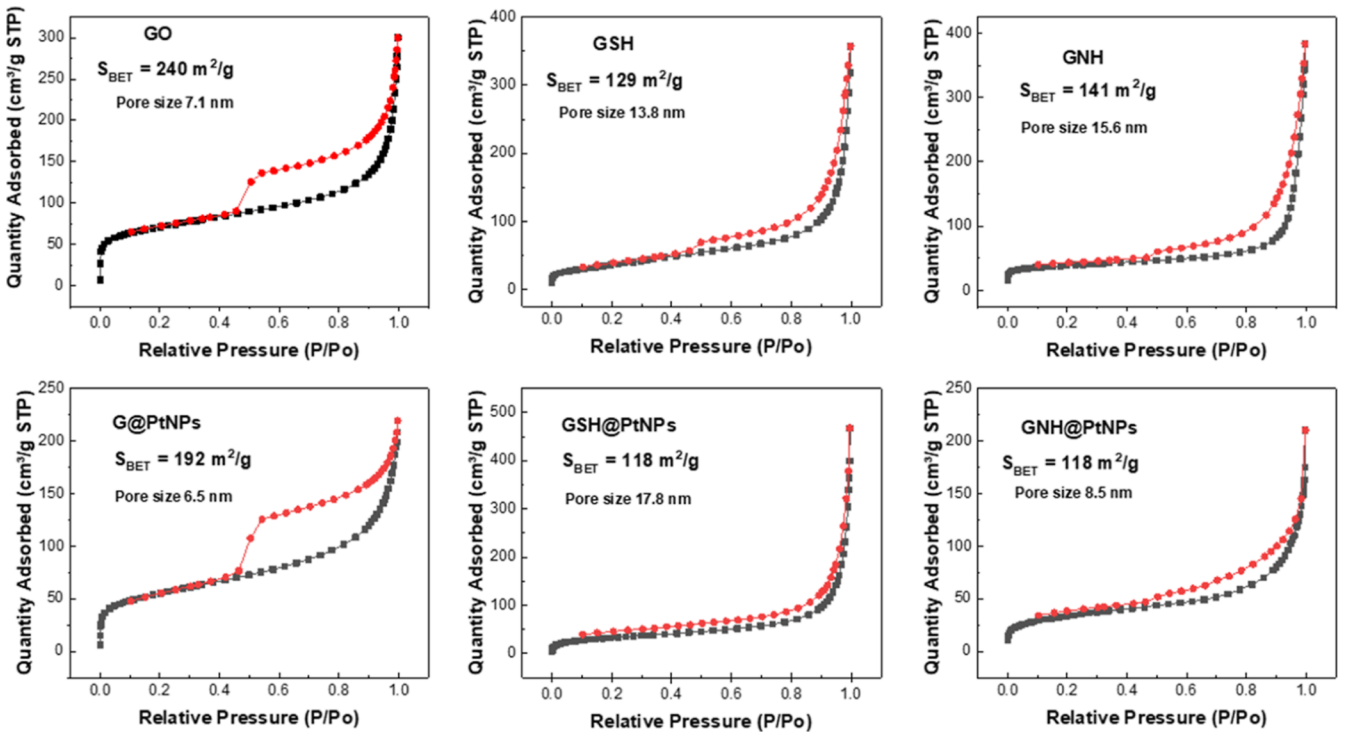

Figure 7. Nitrogen adsorption−desorption curves.

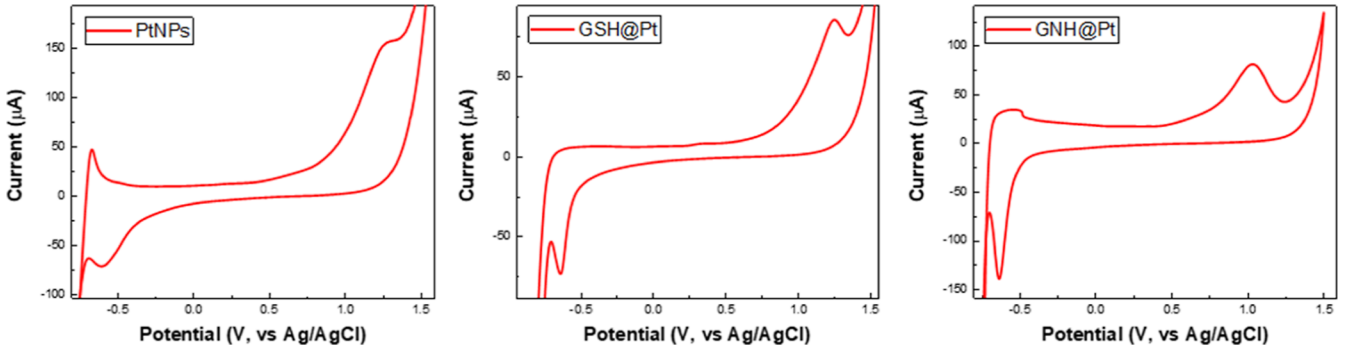

Figure 8. Cyclic voltammograms recorded on electrodes modified with Pt-based catalysts in 0.5 M H_2SO_4.

based anchoring sites in the functionalized carbon supports has promoted uniformity of the metal catalyst.[13,46,47] Also, the high density of nucleophile defects in functionalized carbon supports might lead to an increase in the number of unsaturated carbon atoms,[48] thus facilitating the adsorption of oxygen containing moieties[49,50] and then improving the current responses recorded during MOR.

With thiolated graphene oxide as a supporting layer, the forward peak current (I_f) was increased by 28% and the backward peak current (I_b) was decreased twice (Figure 9B). Consequently, I_f/I_b was increased from 1.72 (for PtNPs/GCE) to 4.35 (for PtNPs@GSH/GCE). At the same time, the position of the oxidation peak in the forward scan was also shifted toward more positive potentials (ΔE = 97 mV). The onset potential was found to have been shifted to a more negative potential by 351 mV ($V_{onset\ (PtNPs)}$ = −143 mV and $V_{onset\ (GSH@PtNPs)}$ = −494 mV). These findings proved that a better CO tolerance and a higher catalytic activity were obtained with the presence of thiolated reduced graphene oxide as the supporting layer. Probably, the dispersion of metal nanoparticles onto a carbonaceous support with a large active area and high density of anchoring sites has been much improved. Especially, the strong Pt−S binding must have significantly contributed to the uniform nucleation of PtNPs on the thiolated carbon support.[51]

Even more, it was found that the MOR is considerably improved on the GNH@PtNP-modified electrode (Figure 9C). At first, it is supposed that MOR forward current should be more significant on the GSH@PtNP-modified electrode due to the high affinity between thiol groups and PtNPs.[35,36] Theoretically, Mallik et al. have also shown a much more efficient catalytic activity on S-doped compared to N-doped graphene.[16] Surprisingly, the forward current obtained on the GNH@PtNP-modified electrode in methanol solution is 20 times higher than that on the GSH@PtNP-modified electrode. However, the onset potential on the GNH@PtNP-modified electrode [$V_{onset\ (GSH@PtNPs)}$ = −397 mV] was found to be comparable with that on the GSH@PtNP-modified electrode [$V_{onset\ (GSH@PtNPs)}$ = −494 mV].

In recently reported studies, it was also found that the modification of carbon supports by using organic molecules containing amino functional groups might help to improve

https://doi.org/10.1021/acs.langmuir.3c01446
Langmuir 2023, 39, 13897−13907

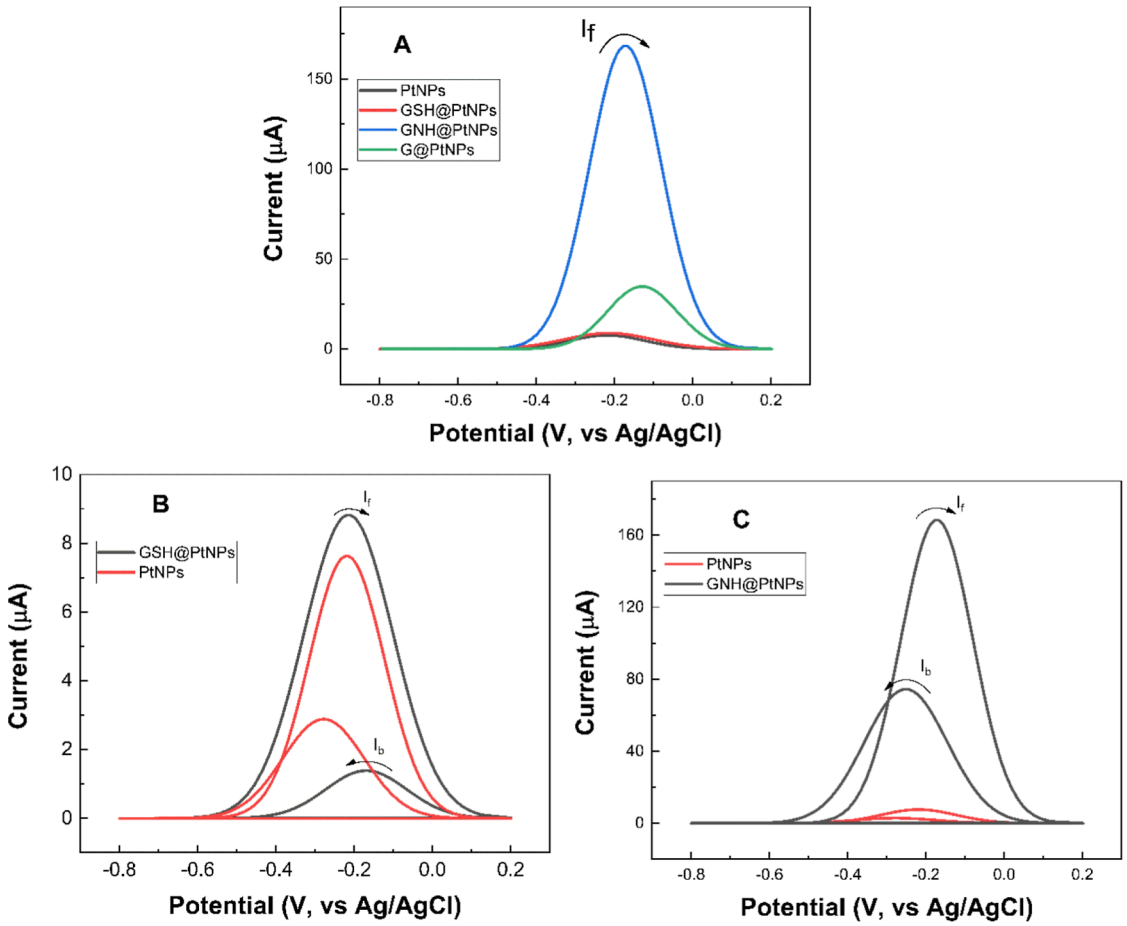

Figure 9. Effect of amine and thiol terminates in carbon supports on MOR effects: (A) forward currents recorded on all electrodes; (B) current responses recorded on the electrode modified with PtNPs and GSH@PtNPs; and (C) current responses recorded on the electrode modified with PtNPs and GNH@PtNPs. All measurements were conducted in 0.5 M KOH solution containing 0.1 MeOH.

catalytic activity of the catalysts. For instance, Ahmad Aryafar et al. have recently reported that a more uniform dispersion of PtNPs and their better catalytic performance were observed on the reduced graphene oxide support functionalized with natural molecules containing amino groups (melamine and chitosan).[52] Chen et al. have shown a very fast kinetics of methanol oxidation on Pt catalysts dispersed on rGO modified with 3-aminopropyltriethoxysilane (an organic linker with one amine end and one silane end).[53]

Considering the fact that we have obtained too many stacks in SEM images and low water solubility of the GSH sample, we suggest that the amine moieties on the surface of GNH has helped to avoid the restacking of graphene sheets and enlarging the specific surface area, which provide more efficient transport pathways for improving catalytic performances.[10] In previous studies, it was also found that the large surface area is often obtained in N-doped graphene.[48,54,55] Therefore, we have examined the active surface area of the samples using the BET technique (Figure 7). However, it turns out that the specific surface areas for GSH@PtNPs and GNH@PtNPs are quite similar even though the specific surface area of GNH is slightly larger than that in GSH. The specific surface areas (determined from BET measurements) were 240, 141, 129, 118, and 118 $m^2\ g^{-1}$ for GO, GNH, GSH, GNH@PtNPs, and GSH@PtNPs, respectively.

We then examine the ECSA of the samples by recording cyclic voltammograms in an acidic solution (Figure 8). It can be seen from Figure 8 that the hydrogen desorption (in the region of −300 to −700 mV) is pretty weak on the electrode modified with GSH@PtNPs. The charge of the hydrogen adsorption−desorption process (Q_H) was estimated from the integral of the peak area shown in the current vs time plot (Figure S5).[31] The ECSA S_{Pt} was then extracted from hydrogen adsorption−desorption charge as mentioned above (Table 2). It was found that the value of S_{Pt} on GNH@PtNPs

Table 2. Determination of the ECSA

	Q_H (μC)	S_{Pt} (cm^2)	m_{Pt} (μg)
PtNPs	1253.0	5.9668	0.633
GSH@Pt	205.5	0.9785	0.104
GNH@Pt	488.6	2.3269	0.247

is about 2.4× larger than that on GSH@PtNPs. Probably, the large ECSA must have contributed to the enhancement in forward current in the MOR test on the electrode modified with GNH@PtNPs. On the other hand, the mass of PtNPs (estimated from Q_H) on the GNH@PtNP-modified electrode (0.247 μg) was also found to be twice higher than that on the GSH@PtNP-modified electrode (0.104 μg) and three times less than on the electrode modified with only PtNPs (0.633 μg) (Figure S6). It seems that even the amount of Pt on GSH@PtNPs is relatively high (Table 1), but the electro-

https://doi.org/10.1021/acs.langmuir.3c01446
Langmuir 2023, 39, 13897−13907

catalytic activity of the catalyst is significantly limited due to the aggregation of PtNPs on the stacked GSH flakes.

Because oxidation of methanol molecules with using the Pt catalyst is often accompanied by the adsorption of hydroxyl moieties,[5] we wonder that the surface charge of the carbon support might affect to the catalytic activity. The zeta potential was found to be −75.2 and 136.8 mV for GSH and GNH, respectively (Figure S4). The positive charge on the GNH sample might have resulted from C−N^+ fragment as shown in the deconvoluted N 1s spectrum of GNH and GNH@PtNPs (Figure 3). The more positive charge on the aminated carbon support might have helped to improve the adsorption of negatively charged hydroxyl groups, thus facilitating the MOR.

Last but not the least, the reduction of GO during amination is not as efficient as in the thiolation process. Indeed, the O/C ratio in GNH (0.232) is still about 1.9 times higher than that in GSH (0.124) (Table 1). On the other hand, there might still be a considerable amount of oxygen-containing functional groups on the aminated flakes. This is also the reason why the aminated carbon support still remains the flexible structure (as seen in SEM images in Figure 1), but the thiolated carbon support becomes highly compact. Chen et al. have reported that the presence of abundant hydroxyl groups on the carbon support can help to enhance the anti-CO poisoning effect of the Pt catalyst.[56−58] Therefore, we suppose that the partial reduction that left a certain amount of hydroxyl groups on the aminated carbon support might also contribute to improving MOR current responses.

CONCLUSIONS

This work demonstrates a comparative study on catalytic activity of PtNPs dispersed onto aminated and thiolated reduced graphene oxide supports toward MOR for the first time. It was shown that both chemically functionalized carbon supports are beneficial for homogeneous dispersion of metal nanoparticles with a particle size less than 5 nm. Moreover, the Pt catalysts based on functionalized carbon supports become very durable due to the strong coordination between metal and electron donor atoms (S and N). It was found that the aminated carbon support owns a more flexible structure with a larger ECSA than the thiolated one. The surface of aminated carbon flakes also shows more positive charges coming from C−N^+ fragments. As a result, the current density recorded during MOR on GNH@PtNPs is much improved than on GSH@PtNPs. Probably, the proposed material may offer a useful guideline to design novel nanocomposites with beneficial electrocatalytic performance for energy and sensing applications. Further studies to better understand the structural evolution during catalysis should be conducted in the near future. It is also possible to decorate metallic or bimetallic catalysts with highly porous morphologies onto these functionalized carbon supports for enhancing their catalytic activity.

ASSOCIATED CONTENT

Supporting Information

The Supporting Information is available free of charge at https://pubs.acs.org/doi/10.1021/acs.langmuir.3c01446.

Histograms, EDX spectra, elemental analysis, Tauc plots, zeta potential measurements, ECSA calculations, evaluation of mass activity and surface activity, and determination of the MOR effect (PDF)

AUTHOR INFORMATION

Corresponding Author

Vu Thi Thu − *Vietnam Academy of Science and Technology (VAST), University of Science and Technology of Hanoi (USTH), Cau Giay, Hanoi 10000, Vietnam;* orcid.org/0000-0003-1634-5348; Email: thuvu.edu86@gmail.com, vu-thi.thu@usth.edu.vn

Authors

Minh Thu Vu − *Vietnam Academy of Science and Technology (VAST), University of Science and Technology of Hanoi (USTH), Cau Giay, Hanoi 10000, Vietnam*

Thi Thanh Ngan Nguyen − *Vietnam Academy of Science and Technology (VAST), University of Science and Technology of Hanoi (USTH), Cau Giay, Hanoi 10000, Vietnam*

Tran Quang Hung − *Vietnam Academy of Science and Technology (VAST), Institute of Chemistry (IOC), Cau Giay, Hanoi 10000, Vietnam;* orcid.org/0000-0001-9867-9207

Thuan-Nguyen Pham-Truong − *CY Cergy Université, LPPI, Cergy F-95000, France;* orcid.org/0000-0002-7340-7296

Magdalena Osial − *Polish Academy of Sciences, Institute of Fundamental Technological Research, Warsaw 02-106, Poland*

Philippe Decorse − *Université Paris Cité, ITODYS, CNRS, Paris F-75013, France*

Thi Thom Nguyen − *Vietnam Academy of Science and Technology (VAST), Institute of Tropical Technology (ITT), Cau Giay, Hanoi 10000, Vietnam*

Benoit Piro − *Université Paris Cité, ITODYS, CNRS, Paris F-75013, France*

Complete contact information is available at: https://pubs.acs.org/10.1021/acs.langmuir.3c01446

Author Contributions

Dr. V.T.T. was responsible for proposing scientific questions in this work. Ms. V.M.T. was in charge for synthesis and characterization of samples as well as performing MOR tests. Dr. N.T.T.N. and Dr. N.T.T. have supported in morphological (SEM) and structural (EDX, FTIR, Raman) characterizations. Dr. T.Q.H. and Dr. P.T.T.N. have provided many valuable suggestions on performing electrochemical studies of the samples. Dr. M.O. was responsible for capturing TEM images. Dr. P.D. and Prof. B.P. were responsible for XPS analysis of the samples. Prof. B.P. and Dr. V.T.T. were in charge of manuscript preparation.

Notes

The authors declare no competing financial interest.

ACKNOWLEDGMENTS

This research was funded by University of Science and Technology of Hanoi (USTH.AMSN.01/21-23).

ABBREVIATIONS

GO, graphene oxide; GSH, thiolated reduced graphene oxide; GNH, aminated reduced graphene oxide; PtNPs, platinum nanoparticles; MOR, methanol oxidation reaction

REFERENCES

(1) Ramli, Z. A. C.; Shaari, N.; Saharuddin, T. S. T.; Saharuddin, T. Progress and major BARRIERS of nanocatalyst development in direct

methanol fuel cell: A review. *Int. J. Hydrogen Energy* **2022**, *47*, 22114−22146.
(2) Ramli, Z. A. C.; Kamarudin, S. K. Platinum-Based Catalysts on Various Carbon Supports and Conducting Polymers for Direct Methanol Fuel Cell Applications: A review. *Nanoscale Res. Lett.* **2018**, *13*, 410.
(3) Hoang, N. T.; Thuan Nguyen, P. T.; Chung, P. D.; Thu Ha, V. T.; Hung, T. Q.; Nam, P. T.; Thu, V. T. Electrochemical preparation of monodisperse Pt nanoparticles on a grafted 4-aminothiophenol supporting layer for improving the MOR reaction. *RSC Adv.* **2022**, *12*, 8137−8144.
(4) Huang, H.; Wei, Y.; Yang, Y.; Yan, M.; He, H.; Jiang, Q.; Yang, X.; Zhu, J. Controllable synthesis of grain boundary-enriched Pt nanoworms decorated on graphitic carbon nanosheets for ultrahigh methanol oxidation catalytic activity. *J. Energy Chem.* **2021**, *57*, 601−609.
(5) Meng, W.; He, H.; Yang, L.; Jiang, Q.; Yuliarto, B.; Yamauchi, Y.; Xu, X.; Huang, H. 1D-2D hybridization: Nanoarchitectonics for grain boundary-rich platinum nanowires coupled with MXene nanosheets as efficient methanol oxidation electrocatalysts. *Chem. Eng. J.* **2022**, *450*, 137932.
(6) Shu, J.; Li, R.; Lian, Z.; Zhang, W.; Jin, R.; Yang, H.; Li, S. In-situ oxidation of Palladium−Iridium nanoalloy anchored on Nitrogen-doped graphene as an efficient catalyst for methanol electrooxidation. *J. Colloid Interface Sci.* **2022**, *605*, 44−53.
(7) Zhang, K.; Deng, Y.; Wu, Y.; Wang, L.; Yan, L. Prussian-blue-analogue derived FeNi2S4/NiS nanoframes supported by *N*-doped graphene for highly efficient methanol oxidation electrocatalysis. *J. Colloid Interface Sci.* **2023**, *647*, 246−254.
(8) Liu, J.-X.; Liang, X.-L.; Chen, F.; Ding, S.-N. Ultrasensitive amperometric cytosensor for drug evaluation with monitoring early cell apoptosis based on Cu_2O@PtPd nanocomposite as signal amplified label. *Sens. Actuators, B* **2019**, *300*, 127046.
(9) Ham, K.; Chung, S.; Lee, J. Narrow size distribution of Pt nanoparticles covered by an S-doped carbon layer for an improved oxygen reduction reaction in fuel cells. *J. Power Sources* **2020**, *450*, 227650.
(10) Huang, Y.; Wei, Q.; Wang, Y.; Dai, L. Three-dimensional amine-terminated ionic liquid functionalized graphene/Pd composite aerogel as highly efficient and recyclable catalyst for the Suzuki cross-coupling reactions. *Carbon* **2018**, *136*, 150−159.
(11) Kaushal, S.; Kaur, M.; Kaur, N.; Kumari, V.; Singh, P. P. Heteroatom-doped graphene as sensing materials: a mini review. *RSC Adv.* **2020**, *10*, 28608−28629.
(12) Parambhath, V. B.; Nagar, R.; Ramaprabhu, S. Effect of nitrogen doping on hydrogen storage capacity of Palladium decorated graphene. *Langmuir* **2012**, *28*, 7826−7833.
(13) Chao, L.; Qin, Y.; He, J.; Ding, D.; Chu, F. Robust three dimensional N-doped graphene supported Pd nanocomposite as efficient electrocatalyst for methanol oxidation in alkaline medium. *Int. J. Hydrogen Energy* **2017**, *42*, 15107−15114.
(14) Yang, N.; Li, L.; Li, J.; Ding, W.; Wei, Z. Modulating the oxygen reduction activity of heteroatom-doped carbon catalysts via the triple effect: charge, spin density and ligand effect. *Chem. Sci.* **2018**, *9*, 5795−5804.
(15) Zhang, X.; Zhu, J.; Tiwary, C. S.; Ma, Z.; Huang, H.; Zhang, J.; Lu, Z.; Huang, W.; Wu, Y. Palladium Nanoparticles Supported on Nitrogen and Sulfur Dual-Doped Graphene as Highly Active Electrocatalysts for Formic Acid and Methanol Oxidation. *ACS Appl. Mater. Interfaces* **2016**, *8*, 10858−10865.
(16) Priyadarsini, A.; Mallik, B. S. Effects of doped N, B, P, and S atoms on graphene toward oxygen evolution reactions. *ACS Omega* **2021**, *6*, 5368−5378.
(17) Yang, H. B.; Miao, J.; Hung, S.-F.; Chen, J.; Tao, H. B.; Wang, X.; Zhang, L.; Chen, R.; Gao, J.; Chen, H. M.; Dai, L.; Liu, B. Identification of catalytic sites for oxygen reduction and oxygen evolution in N-doped graphene materials: Development of highly efficient metal-free bifunctional electrocatalyst. *Sci. Adv.* **2016**, *2*, No. e1501122.
(18) Nguyen, A. T. N.; Shim, J. H. All carbon hybrid N-doped carbon dots/carbon nanotube structures as an efficient catalyst for the oxygen reduction reaction. *RSC Adv.* **2021**, *11*, 12520−12530.
(19) Bai, J.; Zhu, Q.; Lv, Z.; Dong, H.; Yu, J.; Dong, L. Nitrogen-doped graphene as catalysts and catalyst supports for oxygen reduction in both acidic and alkaline solutions. *Int. J. Hydrogen Energy* **2013**, *38*, 1413−1418.
(20) Zhang, L.; Niu, J.; Li, M.; Xia, Z. Catalytic mechanisms of sulfur-doped graphene as efficient oxygen reduction reaction catalysts for fuel cells. *J. Phys. Chem. C* **2014**, *118*, 3545−3553.
(21) Sun, P. Z.; Xiong, W. Q.; Bera, A.; Timokhin, I.; Wu, Z. F.; Mishchenko, A.; Sellers, M. C.; Liu, B. L.; Cheng, H. M.; Janzen, E.; Edgar, J. H.; Grigorieva, I. V.; Yuan, S. J.; Geim, A. K. Unexpected catalytic activity of nanorippled graphene. *Proc. Natl. Acad. Sci. U.S.A.* **2023**, *120*, No. e2300481120.
(22) Yu, W.; Sisi, L.; Haiyan, Y.; Jie, L. Progress in the functional modification of graphene/graphene oxide: a review. *RSC Adv.* **2020**, *10*, 15328−15345.
(23) Jauhar, A. M.; Hassan, F. M.; Cano, Z. P.; Hoque, M. A.; Chen, Z. Platinum−Palladium core-shell nanoflower catalyst with improved activity and excellent durability for the oxygen reduction reaction. *Adv. Mater. Interfaces* **2018**, *5*, 1701508.
(24) Zhu, W.; Gao, J.; Song, H.; Lin, X.; Zhang, S. Nature of the synergistic effect of N and S co-doped graphene for the enhanced simultaneous determination of toxic pollutants. *ACS Appl. Mater. Interfaces* **2019**, *11*, 44545−44555.
(25) Thomas, H. R.; Marsden, A. J.; Walker, M.; Wilson, N. R.; Rourke, J. P. Sulfur-functionalized graphene oxide by epoxide ring-opening. *Angew. Chem., Int. Ed.* **2014**, *53*, 7613−7618.
(26) Chua, C. K.; Pumera, M. Monothiolation and reduction of graphene oxide via one-pot synthesis: hybrid catalyst for oxygen reduction. *ACS Nano* **2015**, *9*, 4193−4199.
(27) Aguilar-Bolados, H.; Vargas-Astudillo, D.; Yazdani-Pedram, M.; Acosta-Villavicencio, G.; Fuentealba, P.; Contreras-Cid, A.; Verdejo, R.; López-Manchado, M. A. Facile and scalable one-step method for amination of graphene using Leuckart reaction. *Chem. Mater.* **2017**, *29*, 6698−6705.
(28) Zhang, W.; Ma, J.; Gao, D.; Zhou, Y.; Li, C.; Zha, J.; Zhang, J. Preparation of amino-functionalized graphene oxide by Hoffman rearrangement and its performances on polyacrylate coating latex. *Prog. Org. Coat.* **2016**, *94*, 9−17.
(29) Rabchinskii, M. K.; Ryzhkov, S. A.; Kirilenko, D. A.; Ulin, N. V.; Baidakova, M. V.; Shnitov, V. V.; Pavlov, S. I.; Chumakov, R. G.; Stolyarova, D. Y.; Besedina, N. A.; Shvidchenko, A. V.; Potorochin, D. V.; Roth, F.; et al. From graphene oxide towards aminated graphene: facile synthesis, its structure and electronic properties. *Sci. Rep.* **2020**, *10*, 6902.
(30) Thanh, L. C.; Nga, D. T. N.; Lam, N. V. B.; Chung, P. D.; Nhi, L. T. T.; Sinh, L. H.; Thu, V. T.; Lam, T. D. Acetylcholinesterase sensor based on PANi/rGO film electrochemically grown on screen-printed electrodes. *Vietnam J. Chem.* **2021**, *59*, 253−262.
(31) Puglia, M. K.; Bowen, P. K. Cyclic voltammetry study of noble metals and their alloys for use in implantable electrodes. *ACS Omega* **2022**, *7*, 34200−34212.
(32) Pak Hoe, L.; Boaventura, M.; Lagarteira, T.; Kee Shyuan, L.; Mendes, A. Polyol synthesis of reduced graphene oxide supported platinum electrocatalysts for fuel cells: Effect of Pt precursor, support oxidation level and pH. *Int. J. Hydrogen Energy* **2018**, *43*, 16998−17011.
(33) Lagarteira, T.; Delgado, S.; Fernandes, C.; Azenha, C.; Mateos Pedrero, C.; Mendes, A. The role of Pt loading on reduced graphene oxide support in the polyol synthesis of catalysts for oxygen reduction reaction. *Int. J. Hydrogen Energy* **2020**, *45*, 20594−20604.
(34) Rupa Kasturi, P.; Harivignesh, R.; Lee, Y. S.; Kalai Selvan, R. Polyol assisted formaldehyde reduction of bi-metallic Pt-Pd supported agro-waste derived carbon spheres as an efficient electrocatalyst for formic acid and ethylene glycol oxidation. *J. Colloid Interface Sci.* **2020**, *561*, 358−371.

https://doi.org/10.1021/acs.langmuir.3c01446
Langmuir 2023, 39, 13897−13907

(35) Chen, F.; Li, X.; Hihath, J.; Huang, Z.; Tao, N. Effect of anchoring groups on single molecule conductance: Comparative study of thiol, amine, and carboxylic acid terminated molecules. *J. Am. Chem. Soc.* **2006**, *128*, 15874−15881.
(36) Rao, X.; Tatoulian, M.; Guyon, C.; Ognier, S.; Chu, C.; Abou Hassan, A. A comparison study of functional groups (amine vs thiol) for immobilizing AuNPs on zeolite surface. *Nanomaterials* **2019**, *9*, 1034.
(37) Stankovich, S.; Dikin, D. A.; Piner, R. D.; Kohlhaas, K. A.; Kleinhammes, A.; Jia, Y.; Wu, Y.; Nguyen, S. T.; Ruoff, R. S. Synthesis of graphene based nanosheets via chemical reduction of exfoliated graphite oxide. *Carbon* **2007**, *45*, 1558−1565.
(38) Velasco-Soto, M. A.; Perez-Garcia, S. A.; Alvarez-Quintana, J.; Cao, Y.; Nyborg, L.; Licea-Jimenez, L. Selective bandgap manipulation of graphene oxide by its reduction with mild reagents. *Carbon* **2015**, *93*, 967−973.
(39) Abid, P. S.; Sehrawat, P.; Islam, S. S.; Mishra, P.; Ahmad, S. Reduced graphene oxide (rGO) based wideband optical sensor and the role of temperature, defect states and quantum efficiency. *Sci. Rep.* **2018**, *8*, 3537.
(40) Bhatnagar, D.; Singh, S.; Yadav, S.; Kumar, A.; Kaur, I. Experimental and theoretical investigation of relative optical band gaps in graphene generations. *Mater. Res. Express* **2017**, *4*, 015101.
(41) Chakraborti, H.; Bramhaiah, K.; John, N. S.; Pal, S. K. Excited state electron transfer from aminopyrene to graphene: a combined experimental and theoretical study. *Phys. Chem. Chem. Phys.* **2013**, *15*, 19932.
(42) Huang, H.; Li, Z.; She, J.; Wang, W. Oxygen density dependent band gap of reduced graphene oxide. *J. Appl. Phys.* **2012**, *111*, 054317.
(43) Mathkar, A.; Tozier, D.; Cox, P.; Ong, P.; Galande, C.; Balakrishnan, K.; Reddy, A. L. M.; Ajayan, P. M. Controlled, stepwise reduction and bandgap manipulation of graphene oxide. *J. Phys. Chem. Lett.* **2012**, *3*, 986−991.
(44) Lian, K.-Y.; Ji, Y.-F.; Li, X.-F.; Jin, M.-X.; Ding, D.-J.; Luo, Y. Big bandgap in highly reduced graphene oxides. *J. Phys. Chem. C* **2013**, *117*, 6049−6054.
(45) Tuinstra, F.; Koenig, J. L. Raman spectrum of graphite. *J. Chem. Phys.* **1970**, *53*, 1126−1130.
(46) Sun, Q.; Kim, S. Synthesis of nitrogen-doped graphene supported Pt nanoparticles catalysts and their catalytic activity for fuel cells. *Electrochim. Acta* **2015**, *153*, 566−573.
(47) Kanninen, P.; Luong, N. D.; Sinh, L. H.; Florez-Montano, J.; Jiang, H.; Pastor, E.; Seppala, J.; Kallio, T. Highly active platinum nanoparticles supported by nitrogen/sulfur functionalized graphene composite for ethanol electro-oxidation. *Electrochim. Acta* **2017**, *242*, 315−326.
(48) Tajabadi, M. T.; Basirun, W. J.; Lorestani, F.; Zakaria, R.; Baradaran, S.; Amin, Y. M.; Mahmoudian, M. R.; Rezayi, M.; Sookhakian, M. Nitrogen-doped graphene - silver nanodendrites for the non-enzymatic detection of hydrogen peroxide. *Electrochim. Acta* **2015**, *151*, 126−133.
(49) Chen, Z.; Mou, K.; Wang, X.; Liu, L. Nitrogen-doped graphene quantum dots enhance the activity of Bi_2O_3 nanosheets for electrochemical reduction of CO_2 in a wide negative potential region. *Angew. Chem.* **2018**, *130*, 12972−12976.
(50) An, M.; Du, L.; Du, C.; Sun, Y.; Wang, Y.; Yin, G.; Gao, Y. Pt nanoparticles supported by sulfur and phosphorus co-doped graphene as highly active catalyst for acidic methanol electrooxidation. *Electrochim. Acta* **2018**, *285*, 202−213.
(51) Wang, R.; Higgins, D. C.; Hoque, M. A.; Lee, D.; Hassan, F.; Chen, Z. Controlled Growth of Platinum Nanowire Arrays on Sulfur Doped Graphene as High Performance Electrocatalyst. *Sci. Rep.* **2013**, *3*, 2431.
(52) Aryafar, A.; Ekrami-Kakhki, M.-S.; Naeimi, A. Enhanced electrocatalytic activity of Pt-SnO2 nanoparticles supported on natural bentonite-functionalized reduced graphene oxide-extracted chitosan from shrimp wastes for methanol electro-oxidation. *Sci. Rep.* **2023**, *13*, 3597.
(53) Chen, Y.; Ma, Y.; Zhou, Y.; Huang, Y.; Li, S.; Chen, Y.; Wang, R.; Tang, J.; Wu, P.; Zhao, X.; Chen, C.; Zhu, Z.; Chen, S.; Cheng, K.; Lin, D. Enhanced methanol oxidation on PtNi nanoparticles supported on silane-modified reduced graphene oxide. *Int. J. Hydrogen Energy* **2022**, *47*, 6638−6649.
(54) Zhao, L.; Sui, X.-L.; Li, J.-Z.; Zhang, J.-J.; Zhang, L.-M.; Huang, G.-S.; Wang, Z.-B. Supramolecular assembly promoted synthesis of three-dimensional nitrogen doped graphene frameworks as efficient electrocatalyst for oxygen reduction reaction and methanol electro-oxidation. *Appl. Catal., B* **2018**, *231*, 224−233.
(55) Long, D.; Li, W.; Ling, L.; Miyawaki, J.; Mochida, I.; Yoon, S.-H. Preparation of nitrogen—doped graphene sheets by a combined chemical and hydrothermal reduction of graphene oxide. *Langmuir* **2010**, *26*, 16096−16102.
(56) Chen, G.; Dai, Z.; Bao, H.; Zhang, L.; Sun, L.; Shan, H.; Liu, S.; Ma, F. Enhanced Anti-CO poisoning of platinum on mesoporous carbon spheres by abundant hydroxyl groups in methanol electro-oxidation. *Electrochim. Acta* **2020**, *336*, 135751.
(57) Zhao, J.; Zeng, H.; Lu, Z.-X. Pt nanowires on monolayered graphene oxide for electrocatalytic oxidation of methanol. *ACS Appl. Nano Mater.* **2022**, *5*, 13594−13600.
(58) Salarizadeh, P.; Askari, M. B.; Di Bartolomeo, A. MoS_2/Ni_3S_2/reduced graphene oxide nanostructure as an electrocatalyst for alcohol fuel cells. *ACS Appl. Nano Mater.* **2022**, *5*, 3361−3373.

https://doi.org/10.1021/acs.langmuir.3c01446
Langmuir 2023, 39, 13897−13907